



Multi-Temporal Hyperspectral and Radar Remote Sensing for Estimating Winter Wheat Biomass in the North China Plain

WOLFGANG KOPPE, MARTIN L. GNYP, Köln, SIMON D. HENNIG, Friedrichshafen, FEI LI, YUXIN MIAO, XINPING CHEN, Peking, China, LIANGLIANG JIA, Shijiazhuang, China & GEORG BARETH, Köln

Keywords: SAR, hyperspectral imaging, vegetation indices, multi-spectral, biomass

Summary: This paper illustrates the results obtained in the frame of experimental campaigns carried out on winter wheat fields in the North China Plain from March 2006 to June 2007. Investigations focused on the methodology of estimating biomass on a regional scale with hyperspectral (EO-1 Hyperion) and microwave data (Envisat ASAR). Special importance is drawn to the combined analysis of microwave and optical satellite data for crop monitoring. Since hyperspectral and synthetic aperture radar (SAR) sensors respond to crop characteristics differently, their complementary information content can support the estimation of crop conditions. During the regular field measurements, satellite data from jointing to ripening stages were acquired. Linear regression models between measured surface reflection as well as surface backscatter and wheat's standing biomass were established. For hyperspectral data, the normalized ratio index (NRI) based on 825 nm and 1225 nm wavebands was calculated from 2006 data as input for the regression model. In addition, Envisat ASAR VV polarization data were related to winter wheat crop parameters. Bivariate correlation results from this study indicate that both multi-temporal EO-1 Hyperion as well as Envisat ASAR data provide notable relationships with crop conditions. As expected, linear correlation of hyperspectral data performed slightly better for biomass estimation ($R^2 = 0.83$) than microwave data ($R^2 = 0.75$) for the 2006 field survey. Based on the results, hyperspectral Hyperion data seem to be more sensitive to crop conditions. Improvements for crop parameter estimation were achieved by combining hyperspectral indices and microwave backscatter into a multiple regression analysis as a function of crop parameters. Combined analysis was performed for biomass estimation ($R^2 = 0.90$) with notable improvements in prediction power.

Zusammenfassung: *Multi-temporale Hyperspektral- und Radarfernerkundung zur Ableitung von Biomasse des Winterweizens in der nordchinesischen Tiefebene.* Ziel der vorliegenden Studie ist die Betrachtung des Potentials multi-temporaler optischer und Radarfernerkundung zur Ableitung der Biomasse des Winterweizens auf regionaler Ebene. Hierzu wurden in der nordchinesischen Tiefebene in den Wachstumsperioden 2006 und 2007 umfangreiche Feldmessungen von Bestandsparametern während der Satellitenüberflüge durchgeführt. Die verwendeten Satellitendaten sind zum einen Hyperspektralradar (EO-1 Hyperion) und zum anderen C-Band Radardaten (Envisat ASAR). Neben der separaten Auswertung von Hyperspektral- und SAR-Daten wurde weiterhin das Synergiepotential aus beiden Aufnahmeverfahren betrachtet. Mit Hilfe von linearen Regressionsmodellen zwischen Satellitendaten und Biomasse wurde die Sensitivität hyperspektraler Reflexion und Radarrückstreuung im Hinblick auf das Wachstum des Winterweizens untersucht. Für die Hyperspektralradar erwies sich der normalized ratio Index (NRI) mit den Wellenlängenbereichen 825 nm und 1225 nm als sensitiv für die Ableitung von Biomasse. Das Modell wurde auf Basis von Daten der Wachstumsperiode 2006 entwickelt und auf die Wachstumsperiode 2007 zur Validierung angewendet. Weiterhin wurde die gemessene Biomasse mit der gleichpolarisierten (VV) C-Band Rückstreuung des Envisat ASAR Sensors linear in Beziehung gesetzt. Als Ergebnis zeigt sich ein deutlicher Zusammenhang zwischen Fernerkundungsdaten und Biomasse, wobei der Regressionskoeffizient deutlich höher für den NRI basierend auf Hyperspektralradar ($R^2 = 0.83$) ausfällt, als der lineare Zusammenhang mit der Radarrückstreuung ($R^2 = 0.75$). Um den komplementären Informationsgehalt von Hyperspektral- und Radardaten zu nutzen, wurde ein multiples Regressionsmodell erstellt, welches eine Verbesserung der Biomasseschätzung ermöglicht ($R^2 = 0.90$).

1 Introduction

China cereal acreage and production is one of the most important in the world, with a crop area of about 88 million ha and production estimated at 483 million tons in 2009, accounting for ca. 22% of total global production (FAO 2011). The North China Plain is one of the most important cereal production regions in China, accounting for almost 50% of China's winter wheat cultivation (NATIONAL BUREAU OF STATISTICS OF CHINA 2010). In agricultural issues, timely monitoring of crop growth status at an early stage is important for in-season site specific crop management, detection of plant vitality as well as assessment of seasonal production at local and regional level (MIAO et al. 2009, LAUDIEN & BARETH 2006).

The sensitivity of the visible (VIS) and near infrared (NIR) reflectance to water content, pigment of the leaves, as well as leaf structure, permits determining indicators for crop conditions (KUMAR et al. 2003). For the linkage of crop parameters with spectral reflectance measurements, a wide range of vegetation indices were developed (ZHAO et al. 2007, BROGE & MORTENSEN 2002). Vegetation indices obtained from spectral reflectance measurements are designed to enhance the vegetation cover signal while minimizing the response of various background materials (SCHOWENGERDT 2007).

Numerous studies have successfully related vegetation indices calculated from the visible and near infrared bands of multispectral scanners with crop parameters such as crop vigour (BROGE & LEBLANC 2000), standing biomass and grain yield (TUCKER 1979, DORALSWAMY et al. 2003). At higher vegetation densities, standard vegetation indices, such as simple ratio (SR) or normalized difference vegetation index (NDVI) are generally less accurate (JONGSCHAAP & SCHOUTEN 2005) and tend to saturate (HABOUDANE et al. 2004, MUTANGA & SKIDMORE 2004), which results in a limited prediction value. To overcome these limitations, hyperspectral vegetation indices for biomass and grain yield prediction have been tested, that are calculated based on all waveband combinations (XAVIER et al. 2006, HANSEN & SCHJOERRING 2003). Narrow band vegetation indices other than standard NDVI were

successfully used for biomass estimation of winter wheat in the North China Plain (KOPPE et al. 2010), which reduces the saturation effect. The same was reported by MUTANGA & SKIDMORE (2004) for pasture biomass estimation. However, DARVISHZADEH et al. (2008) and JAMER et al. (2003) demonstrated that biophysical parameters could be better estimated by multivariate methods such as partial least square regression because 2-channel vegetation indices make only use of a small subset of the available spectral information. Beside the advantages and robustness of vegetation indices for biomass estimation, a drawback is the necessity of reference data for model calibration. Alternative and more complex quantification approaches are physically based radiative transfer models (CHO et al. 2008). These models simulate the hyperspectral signature and remotely sensed data can be used for model recalibration (RICHTER et al. 2009).

Nonetheless, methods based on optical remote sensing are limited in monitoring applications due to cloud cover or daylight dependency. Thus, a monitoring system based only on optical remote sensing would be rather unreliable especially in higher latitudes or in the wet tropics. SAR overcomes the problems of daylight dependency and cloudiness by actively illuminating the earth surface in the wavelength range from a few centimeters to one meter (BRISCO & BROWN 1998). SAR sensors with their all weather capabilities are good remote sensing sources due to their frequent revisits and sensitivity to surface characteristics (KUGLER et al. 2007).

Since the amount of energy backscattered towards the sensor strongly depends on surface roughness and dielectric properties, it is reasonable that SAR can be used for crop type classification, growth stage mapping and biomass monitoring (McNAIRN & BRISCO 2004). For different applications, knowledge of the interaction of the surface characteristics with sensor configurations such as frequency, resolution, incidence angle and polarization is of importance (INOUE et al. 2002). For C-Band SAR measurements, many studies dealt successfully with prediction of standing biomass (BRISCO & BROWN 1998), but the interpretation of the SAR backscatter has proven to be complicated.

There are also investigations on wheat's biomass retrieval based on spaceborne C-band sensors (MATTIA et al. 2003). The results from these studies showed that the backscattering of crops is a complex combination of acquisition parameters (polarization, incidence angle) as well as crop and cultivation characteristics (crop geometry, density, canopy and soil moisture). The combination of these parameters controls the interaction of the incoming electromagnetic wave with the crop canopy and the underlying soil layer.

In the past, quite a few experiments have been performed on wheat fields, either based on spaceborne SAR sensors or on ground-based scatterometers. SATALINO et al. (2009) and BROWN et al. (2003) acquired C-band spaceborne and scatterometer data over wheat fields and found that wheat biomass is strongly related to HH/VV backscatter during the whole growing season. The good performance of the HH/VV ratio is due to the differently attenuated vertically and horizontally polarized waves that propagate through a mainly vertical medium of wheat (PICARD et al. 2003). McNAIRN et al. (2004) differentiated zones of productivity of wheat fields also using scatterometer data. They reasoned that zones of higher productivity had higher backscatter for linear polarizations, with the greatest contrast for HV.

To move towards an operational crop monitoring approach, it is necessary to mitigate the risk associated with reliance on a single source. To meet these requirements and to improve crop parameter estimation and discrimination, methodologies that integrate optical as well as SAR data were developed (BRISCO & BROWN 1995). McNAIRN et al. (2009) performed crop inventories based on multitemporal and multisensoral satellite data with classification improvements of 3 to 18% when adding SAR data to single optical data. Using Envisat ASAR and Landsat TM multispectral images, LIU et al. (2006) achieved a significant improvement for yield estimation by combining both sources in the prediction model.

The synergistic use of different sources was also successfully performed for the integration of hyperspectral optical data with SAR data, mainly for the enhancement of land cover classification based on an image fusion

approach at the pixel level (CHEN et al. 2003, CHANG et al. 2004) and at the feature level (HELD et al. 2003).

In the following study, hyperspectral EO-1 Hyperion data and Envisat ASAR data are combined at the feature level to improve crop parameter estimation in North China Plain.

The main objectives of this paper are: (1) to quantitatively describe C-VV SAR backscattering of winter wheat canopy; (2) to investigate the ability to predict crop standing biomass by Envisat ASAR and EO-1 Hyperion data; (3) to explore the potential of complementary use of SAR and hyperspectral data for mapping crop and field conditions at a regional level.

2 Material and Methods

2.1 Combined Analysis of ASAR and Hyperion Data

The plant parameter estimation for winter wheat consists of separate processing chains for SAR and hyperspectral data in a first step and the combined analysis at the feature level (POHL & VAN GENDEREN 1998) as a second step. The generalized processing chain is illustrated in Fig. 1. The processing of ASAR and Hyperion data contains sensor specific pre-processing steps of the multi-temporal datasets. Subsequent to the pre-processing of the raw data, regression models with the ground truth data were established to estimate the predicting power of remotely sensed data for wheat's plant parameters. Correlation coefficients were calculated for individual hyperspectral indices and SAR backscatter to assess the overall information content of the remotely sensed time series. A further field campaign in 2007 with accompanying EO-1 Hyperion data acquisitions allowed a second validation of established hyperspectral regression models for 2006. Finally, the potential of integrating SAR and hyperspectral data is explored at the feature level for model improvements. Therefore, coefficients of multiple correlations were generated involving hyperspectral indices and SAR backscatter.

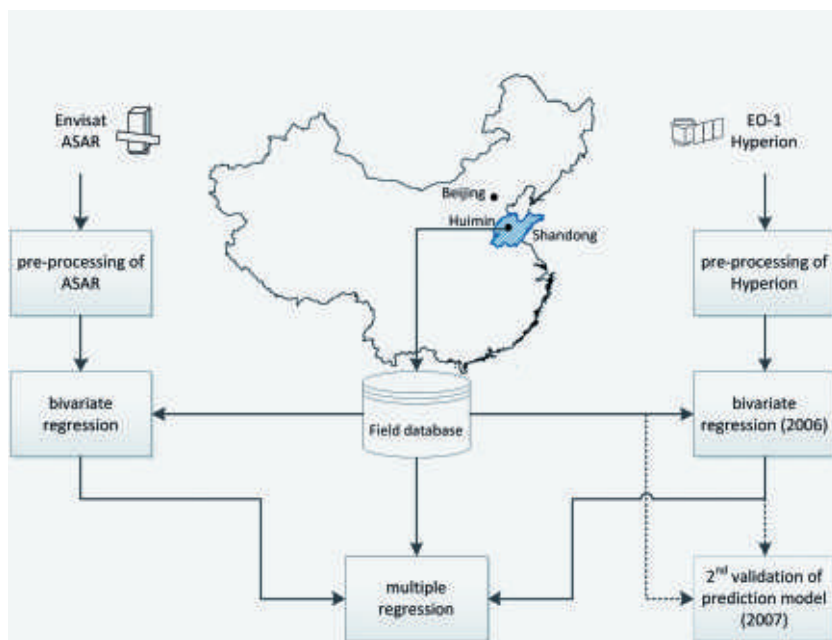


Fig. 1: Area of interest and processing flow for SAR- and hyperspectral derived crop condition estimation.

2.2 Study Area

The test site Huimin County is located in China in the northeast of the Shandong province at around 37.3° N latitude and 117.4° E longitude, which is part of the North China Plain. The area is characterized by a warm temperature sub-humid continental monsoon climate with a mean temperature of around 12.5 °C. The average yearly precipitation sum is approximately 600 mm with a maximum between June and August. The topography of the area is rather flat with an average elevation of around 20 m. In the south of the study site the hills rise up to 400 m.

More than two-thirds of the fields in the study area are cultivated in a crop rotation system with two harvests per year, winter wheat from autumn to June and summer-maize from June to autumn. The cultivation of winter wheat is only possible with irrigation in the dry period of spring.

The investigated crop fields are located around small villages close to the Yellow River in southern Huimin County (Fig. 2). In each year, four fields with an average of around 2.5

to 4.5 ha were selected for regression analysis with satellite data. Two of these four fields were the same in both years. All fields were managed by the farmers in their customary manner. Winter wheat cultivars Jimai20, Jimai21 and Weimai8 were sown from mid of September to beginning of October. Since the fields belong to different farmers, the amount of N-fertilization varies from farmer to farmer. The winter wheat was planted between September and October and harvesting took place between the beginning and mid of June in the following year.

2.3 Ground Truth Data Acquisition

Spectral reflectance and agronomic parameter measurements were taken throughout the growing period of winter wheat from March to June in 2006 and 2007. The measurements were carried out on a regular basis and were synchronized as far as possible with the satellite overpass of EO-1 and Envisat. Field measurements were carried in four villages, Xili, Xujia, Dongjie and Shizhang, whereas four

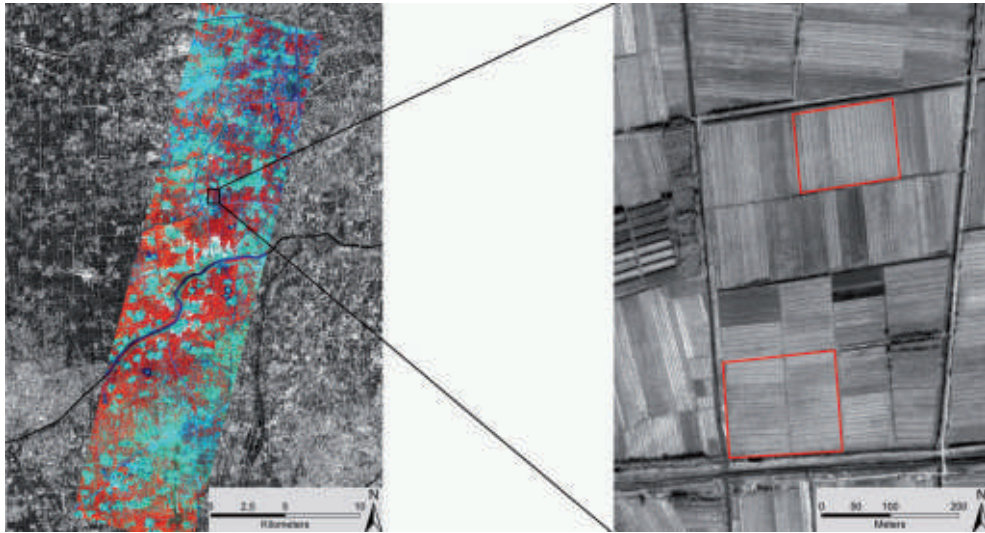


Fig. 2: Left: Envisat ASAR VV (10 May 2006) overlaid by EO-1 Hyperion (R: 823 nm, G: 1638 nm, B: 671 nm, April 19, 2006). Right: Two of the four fields used for ground truth measurements (Background: Ikonos pan image, June 20, 2006).

Tab. 1: Average soil chemical properties of the four fields.

Chemical property	Mean	Min	Max	STD
Total N (g/kg)	0.9	0.6	1.3	0.1
Olsen-P (mg/kg)	32.5	11.3	52.6	11.7
Exchangeable-K (mg/kg)	120.3	65.6	222.0	24.8
Organic matter (g/kg)	13.5	9.5	18.5	1.7

Tab. 2: Crop condition variables mean and standard deviation (STD) measured at different dates in 2006 and 2007.

Date	Growth stage	n*	Biomass dry (kg/sqm)		Plant height (cm)		PWC (%)	
			Mean	STD	Mean	STD	Mean	STD
25 March 2006	Tillering	65	0.06	0.03	11.4	1.9	73.2	1.5
13 April 2006	Jointing	58	0.21	0.05	36.8	2.8	82.3	0.6
19 April 2006	Jointing	63	0.48	0.05	45.0	4.8	83.9	1.4
29 April 2006	Booting	64	0.74	0.09	54.9	5.6	83.5	1.2
10 May 2006	Heading	59	0.96	0.07	74.5	5.5	76.3	1.7
11 April 2007	Jointing	67	0.43	0.04	41.4	4.8	-	-
21 April 2007	Jointing	67	0.62	0.07	64.6	6.0	-	-
6 May 2007	Booting	62	1.05	0.08	93.4	5.8	-	-

* n – measured samples at the different ground truth acquisition days

large fields in total were selected. The fields are each about 2.5 to 4.5 ha in size and subdivided into smaller plots that were managed by different farmers. Two of these fields are shown in Fig. 2 and the average soil chemical properties of the four fields are listed in Tab. 1. In average 63 randomly selected points were sampled at the four fields (around 15 per field) at the different ground truth acquisition days (Tab. 2) to account for spatial variability. At these points, spectral reflection, plant height and destructive biomass measurements were performed. To transfer point measurements to surface data, a continuous surface from the set of points was created by inverse distance weighting method. Taking the different image characteristics of EO-1 Hyperion and Envisat ASAR into account, the sub-plots were prepared in a different way. For EO-1 Hyperion, regression analysis was performed on a pixel basis. After excluding mixed pixel on the field borders, 57 pixel in 2006 and 54 pixel in 2007 remained for further analysis. For Envisat ASAR data, the four fields were separated into homogenous parcels to overcome the speckle effect.

The canopy spectral reflectance measurements were obtained using high resolution spectrometers from Analytical Spectral De-

vices Inc. (ASD). In 2006, a handheld field-spec (range: 325 nm to 1075 nm) was used and in 2007 a QualitySpec (range: 350 nm to 1800 nm). As a new spectrometer covering a wider spectral range was available in 2007, this QualitySpec was used for canopy spectral reflectance measurements. In-situ spectral reflectance measurements were acquired for calibration of satellite hyperspectral data. Contemporaneously with the reflectance measurements, agronomic data were collected for the fields as well. Aboveground biomass was taken destructively by cutting vegetation at ground level within an area of 30 cm by 30 cm. The samples were dried at 70 °C to constant weight. As a result of regular ground truth collection, mean and standard deviation (STD) of biomass, plant height and plant water content (PWC, for 2006) at different growth stages are shown in Tab. 2. Because of favourable weather conditions in 2007 the winter wheat's growing season started earlier.

2.4 Pre-Processing of Hyperspectral and SAR Data

During the first field campaign in 2006, Envisat ASAR data and EO-1 Hyperion data were

Tab. 3: Envisat ASAR and EO-1 Hyperion image acquisition dates and associated crop growth stages.

Satellite	Date of acquisition	Growth stage	Mode	Path direction	Rel. Orbit	Local inc. angle (°)
Envisat ASAR	25 Mar 2006	Tillering	IS5	Ascending	168	39
	13 April 2006	Jointing	IS6	Ascending	440	42
	29 April 2006	Booting	IS6	Ascending	168	39
	10 May 2006	Heading	IS6	Descending	318	40
	3 June 2006	Ripening	IS6	Ascending	168	39
EO-1 Hyperion	19 April 2006	Jointing				
	6 May 2006	Heading				
	31 May 2006	Ripening				
	11 April 2007	Jointing				
	21 April 2007	Booting				
	6 May 2007	Heading				

acquired for the test area. For this study, Envisat ASAR IMP VV intensity precision images with a pixel spacing of 12.5 m and a nominal spatial resolution of 30 m were selected. The imaging modes of the ASAR data were acquired in IS5 and IS6 mode with an incidence angle range between 39° to 42°. To get a larger area covered and to shorten time between acquisitions, different relative orbits were chosen. The four test fields for the recent study are located in the overlapping area of all acquisitions.

The Envisat and Hyperion data were acquired at approximately the same time for the area of interest during the 2006 field campaign. The Envisat and Hyperion acquisitions of the multi-temporal stacks overlap at mid of April (jointing stage) and beginning of May (booting to heading stage). Hyperion data provided 242 bands within the spectral range from 0.4 to 2.5 μm . In addition to the growing season of 2006, three EO-1 Hyperion images were acquired during the growing season of 2007 to validate Hyperion image results from the previous year. The list of acquired Envisat ASAR and EO-1 Hyperion images is presented in Tab. 3.

EO-1 Hyperion Data

The Hyperion sensor is mounted on the Earth Observing One (EO-1) Satellite platform that follows the World Reference System-2 (WRS-2) with a 16 day repeat cycle for nadir mode. It acquires data in a 4.5 km by 100 km footprint with 30 m resolution. Pre-processing of the satellite images from Hyperion is necessary to improve the quality for multi-temporal data analysis. The processing includes the correction of artifacts introduced by the sensor, atmospheric correction and geometric correction (KHURSHID et al. 2006).

For Hyperion, a Flag-Mask indicating sensor and processing artifacts was delivered with the data product. During correction of sensor artifacts, 101 of the 242 hyperspectral bands were excluded using ENVI software (ITT VISUAL INFORMATION SOLUTIONS 2011).

Atmospheric correction is an important step when using satellite data for multi-temporal analysis and for relating satellite imagery to ground truth data, for instance with

data from portable spectrometers. At sensor radiance of EO-1 Hyperion data are conditioned by (a) surface reflectance and (b) by atmospheric scatters, caused by water vapour and aerosols (CAIRNS 2003). The correction of atmospheric effects was carried out with the MODTRAN-based radiative transfer algorithm (BERK et al. 2000), which converts the at-sensor radiance to surface reflectance using ENVI's FLAASH module (ITT VISUAL INFORMATION SOLUTIONS 2011). As the standard atmosphere used in the radiative transfer algorithm does not exactly reflect conditions at the time of acquisition, it was necessary to calibrate initial reflectance with in-situ spectrometer measurements.

Geometric correction of satellite images is necessary for spatially related problems and for overlaying data from different sources. Good orthorectification results were achieved by using the sensor model, ground control points (GCPs) and a digital elevation model (SRTM). In the present work 25 GCPs, which were evenly distributed over the area of interest, were used for the orthorectification. A cubic convolution interpolation with a filter kernel of 3x3 was applied during resampling. The results were validated using 20 independent GCPs, and an overall RMSE of ~ 0.5 pixels (15 m) for the location accuracy after orthorectification was achieved. For subsequent regression analysis with ground truth data, the spectral profile for each pixel of the test fields of 2006 and 2007 was extracted.

Envisat ASAR Data

Prior to data analysis, Envisat ASAR images were pre-processed in a four step approach. At first, the image DN were converted to averaged backscattering intensity (dB, squared amplitude) expressed in sigma nought. The normalization of the ASAR images facilitated the multitemporal backscatter analysis of the winter wheat. Based on the header file information and an elevation model, the ASAR images can be converted to sigma nought as follows (ROSICH & MEADOWS 2004):

$$\sigma_{ij}^0 [dB] = 10 * \log_{10} \left(\frac{DN_{ij}^2}{K} \sin(\alpha_{ij}) \right) \quad (1)$$

Where DN is the pixel intensity of the i, j pixel, K the absolute calibration constant and α the incidence angle of the i, j pixel. Finally, sigma nought values were transformed to logarithmic scale. After normalization, the images were co-registered. The first acquisition was defined as the master and subsequent images were treated as slaves and were co-registered to the master image. Next, speckle noise caused by interference of different elementary scatterers was filtered by a 3×3 gamma adaptive filter which showed acceptable results for the tradeoff between edge preservation and speckle reduction. The reduction of the noise level was evaluated by visual inspection and statistical measurement of effective number of looks (ENL) as suggested by OLIVER & QUEGAN (2004):

$$ENL = \frac{\mu^2}{\sigma^2} \quad (2)$$

Where μ is mean value and σ the standard deviation of the measured area. ENL is obtained by calculating the mean and variance intensity over a homogenous area. The higher the value of the quotient the lower the speckle noise in the area. The gamma map filter with a 3×3 kernel yielded an ENL of 29 compared to around 15 of the noisy images.

In a last step, the co-registered and calibrated image stack was georeferenced using well distributed GCPs. The residual error was 0.6 pixel in range and 0.9 pixel in azimuth direction. The test parcels, for which ground truth measurement was performed, were buffered by a one-pixel zone in order to exclude pixels near the boundaries since they could contain information from neighbouring fields.

In order to investigate the temporal backscatter behaviour of wheat as well as for regression analysis, the four fields were separated into six parcels depending on management practice. The fields were the same as for EO-1 Hyperion data analysis in 2006. To overcome random noise (speckle), pixel values of each parcel (around 60 pixel per parcel) were averaged and the multi-temporal SAR signature was generated. Pre-processing procedure was used to prepare ASAR data for multitemporal regression analysis.

3 Results and Discussion

The synergetic use of hyperspectral and radar data for crop monitoring is useful because of its complementary information content. Hyperspectral data provide a high spectral resolution to enhance monitoring of plant biophysical characteristics (KUMAR et al. 2003) and SAR data contribute surface texture and dielectric information (WOODHOUSE 2006) to the combined analysis.

3.1 Temporal Backscatter Behaviour of Winter Wheat

Averaged backscatter values of Envisat ASAR VV were extracted over crop fields in the test area. Fig. 3 shows the temporal variation of winter wheat and bare field backscattering coefficient σ^0 of ASAR VV expressed in decibel. In the box plot, the centre horizontal line marks the median of the sample and the length of each box shows the range of the central 50% of the sample. In general, as the crop grows the number of leaves and the stem height increases, resulting in a corresponding increase in ground cover. This causes an increase in volume backscattering due to the increase of canopy constituents of wheat.

At the beginning of the growing season in March, when stem height of wheat was about 9 to 13 cm, the VV backscatter of wheat fields is close to the backscatter from bare soil. The backscatter from ploughed fields is still higher, since soil surface roughness is higher than for the sowed fields. Similar observations were described by McNAIRN et al. (2009) during the beginning of the growing season. At this growing stage, the backscatter is mainly driven by soil moisture and roughness parameters. When the crop is in the jointing stage on April 13 (stem height between 30 and 40 cm), the backscatter is significantly lower than at the tillering stage (decrease of about 4.5 dB), indicating a strong attenuation of the soil's backscatter by the wheat plants. As the wheat continued to grow through the stages jointing to ripening, the observed backscatter gradually increased by about 3 dB. This suggests a change in the dominant scattering mechanism from soil and roughness backscattering

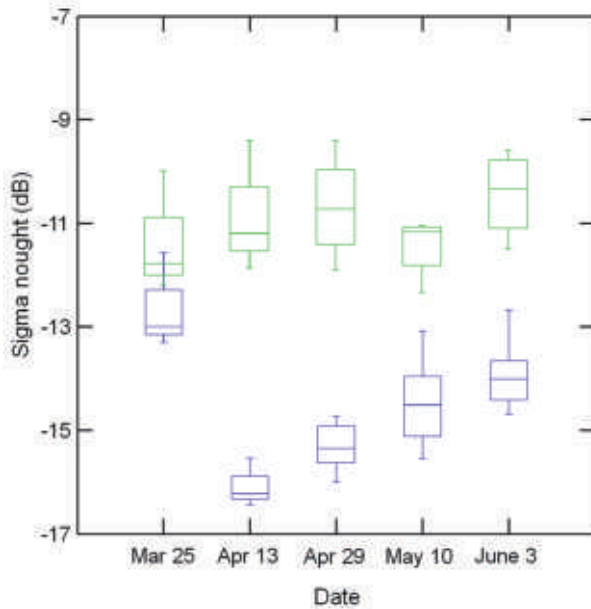


Fig. 3: Temporal C-VV backscatter characteristics of bare soil (green) and winter wheat (blue).

to canopy volume scattering, which is in coincidence with the findings of MATTIA et al. (2003), who mentioned a change in scattering mechanism from soil to volume scattering for incidence angles greater than 40° of fully developed wheat. Also an integral equation method (IEM) simulation carried out by STILES et al. (2000) verified a lower sensitivity of higher incidence angles of VV polarization to soil properties.

In comparison to our observation of an increase in backscatter that begins at a stem height of 35 cm for VV polarization, KARJALAINEN et al. (2008) reported a gradual increase in backscatter for cross-polarization images that does not begin until a stem height of 50 cm is reached.

At the end of the growing season, the water content of plants decreases, while the contribution of soil and surface roughness upon the SAR backscatter increases. As the last Envisat data acquisition was in the ripening stage of the plant, the increase in backscatter from mid of May (heading) to beginning of June (ripening) is also influenced by the soil component. Looking at the backscatter curve of bare fields, a similar increase as for the crop canopy is visible.

The results of field data and backscatter analysis show that the peak of volumetric moisture within the canopy (jointing) did not necessarily coincide with the peak in backscatter (Tab.2 and Fig.3). Besides volume scattering, the interactions between ground and stem for fully developed wheat seem to have an important contribution to the cumulative backscatter value, as also mentioned by PICARD et al. (2003).

Considering the whole vegetation period, the range of backscatter of about 3 dB is lower than measured by KARJALAINEN et al. (2008), but comprehensible if findings by MCNAIRN et al. (2004) are taken into account. They detected a higher sensitivity of HV polarization to crop condition than for VV polarization.

During the growing season, the volumetric soil moisture was relatively constant (between 15 and 30%), thus the change in backscatter of about 3 dB on average of the test parcels was most likely caused by the accumulation of aboveground biomass. Despite the usage of different orbits with slightly different local incidence angles, a dependence of the backscattered signal on incidence angle could not be observed. A strong impact on radar backscatter based on incidence angle differences of

about 5–6° was reported by BAN & HOWARTH (1998).

3.2 Temporal Reflection Behaviour of Winter Wheat

By using the results from regular in-situ spectral reflectance measurements with QualitySpec (ASD) in 2007, the reflectance characteristic of winter wheat during the growing season was compared to spectral measurements of EO-Hyperion. The energy reflected by plants is correlated with crop conditions such as growth stage and nutrient supply. Throughout the measurements from jointing to ripening stage, the reflectance behaviour alters due to structural changes as well as changes in foliar pigments (KUMAR et al. 2003). Up to heading stage the reflectance in the red spectrum (0.65 to 0.7 μm) decreases, which is due to increasing absorption by foliar pigments in the red spectrum. Compared to this, reflectance in the near infrared (NIR) increases caused by

the fast development of plants structural components (THENKABAIL et al. 2000). The 2006 EO-1 Hyperion data is in good consistence with in-situ field spectrometer measurements (KOPPE et al. 2010) due to good atmospheric conditions during the satellite overpass. Fig. 4 shows the spectral average of all fields determined by QualitySpec (red line) and EO-1 Hyperion (blue line) data for 2007. Based on the overlay it can be stated that atmospheric correction performed well; the course of both reflectance curves at a given date are similar in a certain range. Differences can be observed on April 11 and April 21 in the visible and near infrared parts of the spectrum. For these dates hazy conditions with different spatial intensities affected the acquisitions. As a consequence the high absorption (VIS) and maximum reflection (NIR) parts of the spectra are more damped. Especially in the VIS the spectra differ significantly. This part of the electromagnetic spectrum is particularly affected by hazy atmospheric conditions (KUMAR et al. 2003), and atmospheric correction of the

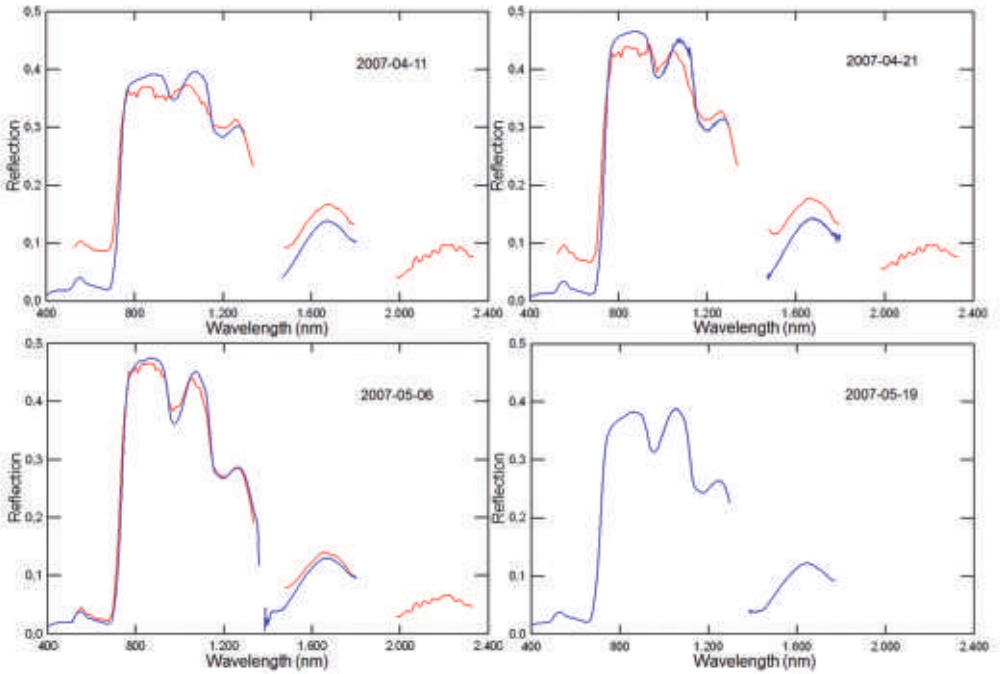


Fig. 4: Averaged reflection behaviour of winter wheat recorded by QualitySpec (blue) and EO-1 Hyperion (red) in the growing season of 2007.

scenes phased problems. For the last satellite acquisition at the beginning of May the measured spectra fits to the in-situ measurements.

The maximum reflectance difference between red and NIR is reached at the end of April (booting). With the beginning of May, the divergence of red and NIR reflectance decreases again. A slightly different behaviour of spectral reflectance is recorded between NIR (875 nm) and SWIR (1225 nm). The divergent trend between the two wavelengths continues up to the heading stage (beginning of May) which delays the saturation effect of crop parameter estimation at full canopy cover (MUTANGA & SKIDMORE 2004). At the mid of May the reflection in NIR is strongly decreasing due to senescence (Fig. 4, lower right). The linear relationship of normalized ratio index (NRI) with biomass is lost at this time.

3.3 Relating Plant Parameters to ASAR and Hyperion Images

Tab. 4 shows the used input data and the relationships between the hyperspectral index (NRI) and ASAR backscatter (C-VV) with standing biomass. Furthermore, the root-mean-square error (RMSE) and relative error (RE) for the regression models are listed. The results of bivariate and multiple correlation analysis will be explained below.

Relating Crop Condition to Envisat ASAR

The sensitivity of Envisat ASAR signals was analyzed as a function of wheat field characteristics. Based on the averaged backscatter values per parcel and the corresponding measured biomass (dry matter) values, a linear regression equation was derived. The bivariate correlation based on linear regression between SAR backscatter and standing biomass resulted in $R^2 = 0.75$ and $RMSE = 0.24 \text{ kg/m}^2$ (Fig. 5 and Tab. 4). The equation of the regression is:

$$BIOM_{2006} = 1.36(VV_{2006}) - 16.3 \quad (3)$$

The coefficient of determination suggests that Envisat ASAR multitemporal imagery is sensitive to crop condition during the growing season of winter wheat.

In an agricultural environment, the monitoring and prediction of biomass and grain yield is one of the most important objectives. Fig. 5 shows that biomass is significantly positively correlated with C-VV backscatter over the growing season with a dynamic range of around 3 dB. At the different dates, the measured sub-plots vary between three and seven, caused by missing measurements at day of ground truth acquisition. For the relationship of C-VV backscatter to biomass, MATTIA et al. (2003) also found an increase in back-

Tab. 4: Input data for model calculation and correlation coefficients between standing biomass and satellite data (2006), for 2007 correlation coefficient between predicted biomass and measured biomass.

Year	Input data typ	Input acquisitions (date)	n*	Correlation coefficients (R2)	RMSE (kg/sqm)	RE (%)
2006	hyperspectral	Apr 19, May 6	114	0.83	0.11	16.1
2006	SAR	Apr 13, Apr 29, 10 May, Jun 3	23	0.75	0.24	25.5
2006	hyperspectral / SAR	19 April, 6 May / Apr 13, Apr 29, May 10, Jun 3	92	0.9	0.81	12.2
		Apr 11, Apr 21, May 6	113	0.84	0.12	17.2
2007	hyperspectral	Apr 11	41	0.19	0.18	45.5
		Apr 21	33	0.58	0.18	29.8
		May 6	39	0.42	0.22	18.2

* n – number of used samples

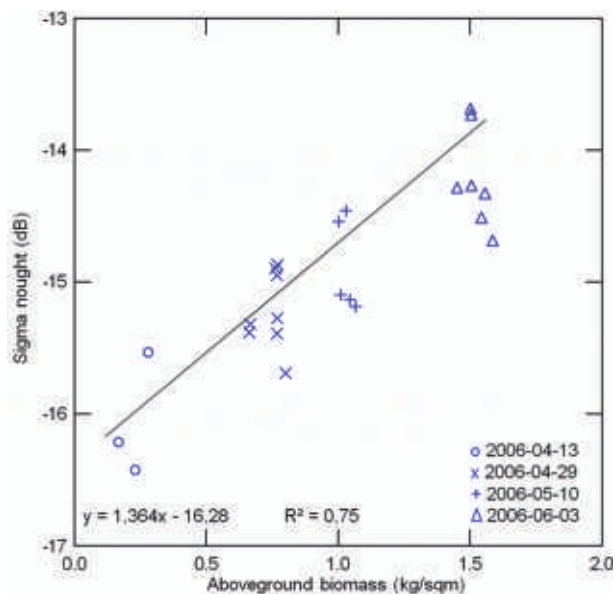


Fig. 5: C-VV backscatter related to aboveground biomass.

scatter following the increase in biomass, but only until the heading stage. After the heading stage, backscatter again decreases which was explained by a change in canopy geometry during heading and booting stage (McNAIRN et al. 2004). At the same phenological stages, LIU et al. (2006) reported a negative correlation of backscatter with biomass and explained this phenomenon also with changes in crop canopy. However, observations of KARJALAINEN et al. (2008) also show a congenerous increase of backscatter with an accumulation of wheat biomass until the heading stage as observed in this study. Beside the positive multi-temporal relationship between biomass and VV backscatter, it is also obviously that in this case microwave is not suitable for prediction of biomass at a given date (mono-temporal). This may be due to less sub-plots which reduces the random sample and dynamic biomass range.

Relating Crop Conditions to EO-1 Hyperion

Based on the studies of SCHOWENGERDT (2007) and THENKABAIL et al. (2000), all possible two-band combinations from the multi-temporal Hyperion data of 2006 (April 19 and May 6)

were calculated according to (4). The last acquisition of Hyperion (May 30) was excluded from the analysis, because senescence has already started. The aim was to determine the best two NRI wavebands for wheat biomass estimation in the North China Plain.

$$NRI_{(band1,band2)} = \frac{(\rho_{band1} - \rho_{band2})}{(\rho_{band1} + \rho_{band2})} \quad (4)$$

$band1 \geq band2$

For the total number of 9870 calculated NRIs, a correlation matrix between standing biomass and two-band vegetation indices was established. In this correlation matrix, wavelengths with high sensitivity to crop condition were detected. For estimation of standing biomass the waveband of 875 nm combined with 1225 nm proved to be most suitable (KOPPE et al. 2010). Similar approaches for different types of vegetation cover showed that band combinations of the red edge (ZHAO et al. 2007) as well as NIR or SWIR (MUTANGA & SKIDMORE 2004, XAVIER et al. 2006) provided a close relationship with LAI and aboveground biomass. These approaches performed much better than spectral bands used in standard vegetation indices. Based on the best waveband combination, a model for biomass esti-

mation was established which resulted in a coefficient of determination (R^2) of 0.83 and a RMSE of 0.11 kg/m²:

$$BIOM_{2006} = 0.25(NRI_{2006}) - 0.01 \quad (5)$$

In order to prove the stability of the established hyperspectral model for EO-1 Hyperion data during the 2006 growing season (5) a validation analysis using EO-Hyperion data for the 2007 growing season was performed. For this, NRI was calculated based on the same waveband combination (875 nm and 1225 nm) that were used in 2006. The resulting NRI values of acquired hyperspectral images in 2007 (April 11, April 21 and May 6) were used to predict biomass at the acquisition dates. The applied equation is the one developed based on the 2006 data.

The validation result of the model is shown in the 1:1 plot in Fig. 6. The model developed for 2006 is able to predict also accumulated biomass in 2007, which is confirmed by a high coefficient of regression of the 1:1 plot ($R^2 = 0.84$). Furthermore, the result is clustered into three separate point clouds that correspond to the different acquisitions of Hyperion data. The acquisitions from April 11 and April 21 show a slight underestimation of the biomass

in comparison to the last acquisition of May 6. This could be due to atmospheric distortions (haze) that affect the reflection from the surface. The difference between the used Hyperion wavebands (875 nm and 1225 nm) for the April scenes is lower than the four field measurements (Fig. 4). This lower waveband difference results in a lesser NRI that leads to an underestimation of the standing biomass in Fig. 6.

In spite of haze influence during the acquisition of EO-1 Hyperion data in April, the stability of the model established for 2006 and applied to 2007, can be regarded as applicable for winter wheat on regional scales in the North China Plain. Changing the scale from regional to local scale, a successful inter-year validation of the developed regression model using field spectrometer data from two years and different cultural conditions was performed by (Li et al. 2008). These observations suggest an across scale validity of hyperspectral crop parameter estimation models in the North China Plain.

Synergy SAR – Hyperspectral

The correlation results based on a linear regression of wheat crop parameters against

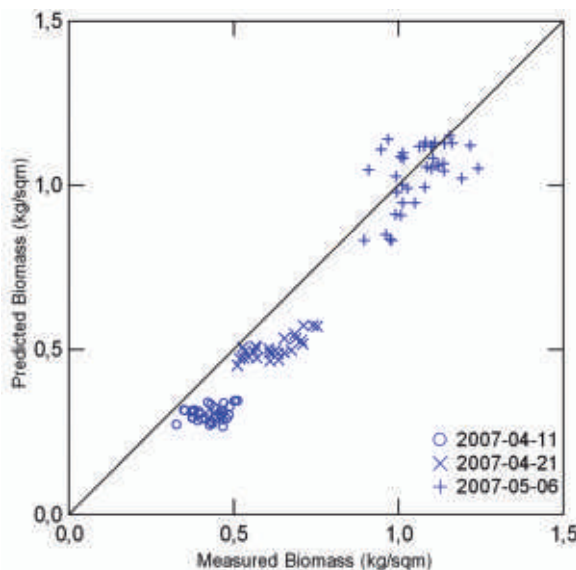


Fig. 6: Measured versus predicted aboveground biomass in 2007 using the regression model developed in (5).

ASAR VV backscatter and NRI calculated from Hyperion data in 2006 show, that crop parameters can be predicted by remotely sensed data from the different acquisition systems. Similar close relationships between crop parameters and satellite data has already been established by THENKABAIL et al. (2004) and XAVIER et al. (2006) for hyperspectral data and furthermore by McNAIRN et al. (2004) for SAR data.

Best results for bivariate correlation were achieved with narrow band vegetation indices derived from EO-1 Hyperion data ($R^2 = 0.83$). Lower coefficients of determination were achieved by using Envisat ASAR backscatter for correlation with crop parameters for the 2006 SAR campaign ($R^2 = 0.75$). If the models derived from SAR and hyperspectral data are combined based on multiplication, the biomass prediction could be improved to $R^2 = 0.90$. The applied equation is:

$$BIOM_{(Hyp/ASAR)} = 2.73(NRI) + 0.16(VV) + 2.68 \quad (6)$$

$(kg\ m^{-2} \quad R^2 = 0.90)$

where $BIOM_{(Hyp/ASAR)}$ is the combined biomass estimate from optical and SAR image analyses, NRI is the normalized ratio index derived from (4) and VV is the ASAR C-VV backscatter. Beside the multiple analysis based on multiplication, there are other types of combination that were not addressed. In this study, the multiple analysis should only demonstrate the improvement of prediction power based on multiple data sources. Similar improvements for yield prediction were achieved by combining time series from SAR and optical data (LIU et al. 2006).

4 Conclusion

This paper describes multitemporal hyperspectral and C-band radar data processing for monitoring winter wheat growth in the North China Plain. Addressing the objectives of this paper stated in the introduction, the following conclusions may be drawn from the research:

1. To achieve high prediction accuracy of wheat's crop parameters based on a single source (ASAR or Hyperion) and combined

analysis of SAR and optical data, it is important to select suitable dates for satellite data acquisition. Based on the satellite multitemporal and multisource data analysis as well as on analysis of field spectrometer data (LI et al. 2008), certain acquisition periods of SAR and hyperspectral data for winter wheat in the North China Plain seem to be convenient. For the acquisition of Hyperion data, the optimized acquisition window is from the beginning of April after tillering to the heading stage before saturation effect of reflectance occurs and flowering begins. In comparison to multispectral imagery, hyperspectral data can improve the performance early and late in the season (XAVIER et al. 2006), which enlarges the acquisition window (STRACHAN et al. 2002). The use of hyperspectral narrow band vegetation indices can reduce saturation effects at the end of the growing season, which was confirmed for winter wheat by KOPPE et al. (2010). For SAR data, observations suggest that a relationship between backscatter and crop parameters can be established between jointing and heading/flowering. Almost similar optimal temporal range from tillering to heading stage for crop parameter estimation is reported by MATTIA et al. (2003) and PICARD et al. (2003).

2. Multitemporal Envisat ASAR VV data at an incidence angle range from 39° to 42° were analyzed as a function of wheat phenological stage. The results show a significant sensitivity to canopy developing stage and a general increasing trend in backscattering with winter wheat growth. However, it is worth mentioning, that there are unsolved problems limiting the value of the results achieved by Envisat ASAR data. First, the resolution of Envisat ASAR is very low compared to the field size, thus only large fields can be included in the analysis. Secondly, the analysis was performed with a small number of fields in a relatively homogenous agricultural environment. Within field and inter-field variation of crop parameters of a specific acquisition date was too low. During the vegetation period, soil moisture remained relatively constant (at least from one acquisition to another), consequently changes in backscatter are due to

- crop growth and less influenced by varying soil moisture.
3. Envisat ASAR C-VV data show certain sensitivity to aboveground biomass. Bivariate regression analysis resulted in a coefficient of determination of about 0.75 for biomass. The simplified relationship between backscatter and crop condition is valid from jointing to heading stage. Before jointing and after heading stage, sophisticated models are necessary to separate backscatter contributions to retrieve canopy parameters. For the relationship of hyperspectral data to crop conditions, narrow band normalized ratio indices based on NIR (875 nm) and SWIR (1225 nm) were calculated for the 2006 growing cycle. As expected, hyperspectral indices show a much higher sensitivity to winter wheat conditions than C-VV radar data. Coefficient of determination was 0.83 for aboveground biomass for multi-temporal approach. To test the validity of the hyperspectral bivariate model, the established model of 2006 was applied to 2007 data to predict aboveground biomass. The predicted vs. measured 1:1 plot resulted in a high coefficient of determination ($R^2 = 0.84$), which proves inter-year validity of hyperspectral prediction power. Compared to multi-temporal approach, single date biomass prediction is more difficult as coefficient of determination is between 0.19 and 0.58 and RMSE is high (Tab. 4). This is caused by lower variability of aboveground biomass across all fields at a given date.
 4. In general, optical and SAR data provide complementary information from a vegetated surface. Hyperspectral sensors record surface reflectance in a wide range of the electromagnetic spectrum which provides the opportunity to extract information about crop canopy parameters and processes at pixel level. SAR microwave penetrate the vegetation and backscatter provide information from inside the canopy. Because of inherent speckle, backscatter values must be spatially averaged for regression analysis. Both kinds of information could be analyzed separately or combined on a feature level. In a final investigation, crop parameters were related to combined C-VV backscatter and hyperspectral indi-

ces by means of a multiple regression model. For the relationship with biomass and plant height, regression models with coefficients of determination of 0.90 for biomass were established. This is an improvement of around 9% for aboveground biomass in comparison to single source hyperspectral regression model. While performance improvement is not that much of a combined model, the synergism of using complementary systems in monitoring winter wheat is obvious. Improvements are more likely to be found in terms of filling acquisition gaps of optical data due to cloud cover and providing additional information by SAR.

References

- BAN, Y. & HOWARTH, P.J., 1998: Orbital effects on ERS-1 SAR temporal backscatter profiles of agricultural crops. – *International Journal of Remote Sensing* **19**: 3465–3470.
- BERK, A., ANDERSON, G.P., ACHARYA, P.K., CHETWYND, J.H., BERNSTEIN, L.S., SHETTLE, E.P., MATTHEW, M.W. & ADLER-GOLDEN, S.M., 2000: MODTRAN4 User's Manual. – Hanscom AFB, MA: Air Force Res. Lab.: 1–93.
- BRISCO, B. & BROWN, R.J., 1995: Multidate SAR/TM synergism for crop classification in western Canada. – *Photogrammetric Engineering and Remote Sensing* **61**: 1009–1014.
- BRISCO, B. & BROWN, R.J., 1998: Agricultural applications with radar. – HENDERSON, F.M. & LEWIS, A.J. (eds.): *Principles and Applications of Imaging Radar*, John Wiley and Sons, New York.
- BROGE, N.H. & LEBLANC, E., 2000: Comparing predicting power and stability of broadband and hyperspectral vegetation indices for estimation of green leaf area index and canopy chlorophyll density. – *Remote Sensing of Environment* **76**: 156–172.
- BROGE, N.H. & MORTENSEN, J.V., 2002: Deriving green crop area index and canopy chlorophyll density of winter wheat from spectral reflectance data. – *Remote Sensing of Environment* **81**: 45–57.
- BROWN, S.C.M., QUEGAN, S., MORRISON, K., BENNETT, J.C. & COOKMARTIN, G., 2003: High-Resolution Measurements of Scattering in Wheat Canopies Implications for Crop Parameter Retrieval. – *IEEE Transactions on Geoscience and Remote Sensing* **41**: 1602–1610.

- CAIRNS, B., 2003: Special Issue Papers – Atmospheric Correction and its Application to an Analysis of Hyperion Data. – *IEEE Transactions on Geoscience and Remote Sensing* **41** (6): 1232–1245.
- CHANG, Y.L., HAN, C.C., REN, H., CHEN, C.T., CHEN, K.S. & FAN, K.C., 2004: Data fusion of hyperspectral and SAR images. – *Optical engineering* **43**: 1787–1797.
- CHO, M.A., SKIDMORE, A.K. & ATZBERGER, C., 2008: Towards red-edge positions less sensitive to canopy biophysical parameters for leaf chlorophyll estimation using properties optique spectrales des feuilles (PROSPECT) and scattering by arbitrarily inclined leaves (SAILH) simulated data. – *International Journal of Remote Sensing* **29** (8): 2241–2255.
- CHEN, C.M., HEPNER, G.F. & FORSTER, R.R., 2003: Fusion of hyperspectral and radar data using the IHS transformation to enhance urban surface features. – *ISPRS Journal of Photogrammetry and Remote Sensing* **59**: 310–322.
- DARVISHZADEH, R., SKIDMORE, A.K., SCHLERF, M., ATZBERGER, C., CORSIA, F. & CHOA, M., 2008: LAI and chlorophyll estimation for a heterogeneous grassland using hyperspectral measurements. – *ISPRS Journal of Photogrammetry and Remote Sensing* **63** (4): 409–426.
- DORALSWAMY, P.C., MOULIN, S., COOK, P.W. & STERN, A., 2003: Crop yield assessment from remote sensing. – *Photogrammetric engineering & remote sensing* **74**: 665–674.
- FAO, 2011: FAO statistical Yearbook, 2011: fao.org/economic/ess/ess-publications/ess-yearbook/ess-yearbook2010/en/ (9.11.2011).
- HABOUDANE, D., MILLER, J.R., PATTEY, E., ZARCO-TEJADA, P.J. & STRACHAN, I.B., 2004: Hyperspectral vegetation indices and novel algorithms for predicting green LAI of crop canopies: Modeling and validation in the context of precision agriculture. – *Remote Sensing of Environment* **90**: 337–352.
- HANSEN, P.M. & SCHJOERRING, J.K., 2003: Reflectance measurement of canopy biomass and nitrogen status in wheat crops using normalized difference vegetation indices and partial least square regression. – *Remote Sensing of Environment* **86**: 542–553.
- HELD, A., TICEHURST, C., LYMBURNER, L. & WILLIAMS, N., 2003: High resolution mapping of tropical mangrove ecosystems using hyperspectral and radar remote sensing. – *International Journal of Remote Sensing* **24**: 2739–2759.
- INOUE, Y., KUROSU, T., MAENO, H., URATSUKA, S., KOZU, T., DABROWSKA-ZIELINSKA, K. & QI, J., 2002: Season-long daily measurements of multi-frequency (Ka, Ku, X, C, and L) and full-polarization backscatter signatures over paddy rice field and their relationship with biological variables. – *Remote Sensing of Environment* **81**: 194–204.
- JAMER, T., KÖTZ, B. & ATZBERGER, C., 2003: Spektroradiometrische Ableitung biophysikalischer Vegetationsparameter von Weizenbeständen: Vergleichende Untersuchung verschiedener empirisch-statistischer Verfahren. – *PFG* **2003** (1): 43–50.
- ITT VISUAL INFORMATION SOLUTIONS, 2011: exelisvis.com/ (15.8.2011).
- JONGSCHAAP, R.W.W. & SCHOUTEN, L.S.M., 2005: Predicting wheat production at regional scale by integration of remote sensing data with a simulation model. – *Agronomy for sustainable development* **25**: 481–489.
- KARJALAINEN, M., KAARTINEN, H. & HYYPPÄ, J., 2008: Agricultural Monitoring Using Envisat Alternating Polarization SAR Images. – *Photogrammetric Engineering & Remote Sensing* **74**: 117–124.
- KHURSHID, K., STAENZ, K., SUN, L., NEVILLE, R., WHITE, H.P., BANNARI, A., CHAMPAGNE, C.M. & HITCHCOCK, R., 2006: Preprocessing of EO-1 Hyperion data. – *Canadian Journal of Remote Sensing* **32**: 84–97.
- KOPPE, W., LI, F., GNYP, M.L., MIAO, Y., JIA, L., CHEN, X., ZHANG, F. & BARETH, G., 2010: Evaluating Multispectral and Hyperspectral Satellite Remote Sensing Data for Estimating Winter Wheat Growth Parameters at Regional Scale in the North China Plain. – *PFG* **2010** (3): 167–178.
- KUGLER, Z., DE GROVE, T., BRAKENRIDGE, T. & ELAINE, A., 2007: Towards a Near-Real Time Global Flood Detection System (GFDS). – 10th International Symposium on Physical Measurements and Signatures in Remote Sensing ISPM-SRS07, GITV BV (Publ.), Davos, Switzerland, Lemmer – JRC37044.
- KUMAR, L., SCHMIDT, K., DURY, S. & SKIDMORE, A., 2003: Imaging spectrometry and vegetation science. – VAN DER MEER, F.D. & DE JONG, S.M. (eds.): *Imaging Spectrometry*, Dordrecht, The Netherlands.
- LAUDIEN, R. & BARETH, G., 2006: Multitemporal Hyperspectral Data Analysis for Regional Detection of Plant Diseases by using a Tractor- and an Airborne-based Spectrometer. – *PFG* **2006** (3): 217–228.
- LI, F., GNYP, M.L., JIA, L., MIAO, Y., YU, Z., KOPPE, W., BARETH, G., CHEN, X. & ZHANG, F., 2008: Estimating N status of winter wheat using a handheld spectrometer in the North China Plain. – *Field Crops Research* **106**: 77–85.
- LIU, L., WANG, J., BAO, Y., HUANG, W., MA, Z. & ZHAO, C., 2006: Predicting winter wheat condi-

- tion, grain yield and protein content using multi-temporal Envisat ASAR and Landsat TM satellite images. – *International Journal of Remote Sensing* **27**: 737–753.
- MATTIA, F., LE TOAN, T., PICARD, G., POSA, F.I., D'ALESSIO, A., NOTARNICOLA, C., GATTI, A.M., RINALDI, M. & SATALINO, G., 2003: Multitemporal C-Band Radar Measurements on Wheat Fields. – *IEEE Transactions on Geoscience and Remote Sensing* **41** (7): 1551–1560.
- McNAIRN, H. & BRISCO, B., 2004: The application of C-band polarimetric SAR for agriculture: a review. – *Canadian Journal of Remote Sensing* **30**: 525–542.
- McNAIRN, H., HOCHHEIM, K. & RABE, N., 2004: Applying polarimetric radar imagery for mapping the productivity of wheat crops. – *Canadian Journal of Remote Sensing* **30**: 517–524.
- McNAIRN, H., CHAMPAGNE, C., SHANG, J., HOLMSTROM, D. & REICHERT, G., 2009: Integration of optical and synthetic aperture radar (SAR) imagery for delivering operational annual crop inventories. – *ISPRS Journal of Photogrammetry and Remote Sensing* **64**: 434–449.
- MIAO, Y., MULLA, D.J., RANDALL, G.W., VETSCH, J.A. & VINTILA, R., 2009: Combining chlorophyll meter readings and high spatial resolution remote sensing images for in-season site-specific nitrogen management of corn. – *Precision Agriculture* **10**: 45–62.
- MUTANGA, O. & SKIDMORE, A.K., 2004: Narrow band vegetation indices overcome the saturation problem in biomass estimation. – *International Journal of Remote Sensing* **25**: 3999–4014.
- NATIONAL BUREAU OF STATISTICS OF CHINA, 2010: China agriculture yearbook. – 258 p., China Agriculture Press.
- OLIVER, C. & QUEGAN, S. (ed.), 2004: Understanding Synthetic Aperture Radar Images. – Sci-Tech, NC 27613.
- PICARD, G., LE TOAN, T. & MATTIA, F., 2003: Understanding C-Band Radar Backscatter From Wheat Canopy Using a Multiple-Scattering Coherent Model. – *IEEE Transactions on Geoscience and Remote Sensing* **41**: 1583–1591.
- POHL, C. & VAN GENDEREN, J.L., 1998: Multisensor image fusion in remote sensing concepts, methods and applications. – *International Journal of Remote Sensing* **19**: 823–854.
- RICHTER, K., ATZBERGER, C., VUOLO, F., WEIHS, P. & D'URSO, G., 2009: Experimental assessment of the Sentinel-2 band setting for RTM-based LAI retrieval of sugar beet and maize. – *Canadian Journal of Remote Sensing* **35** (3): 230–247.
- ROSICH, B. & MEADOWS, P., 2004: Absolute Calibration of ASAR Level 1 Products. Technical Note. – <http://earth.esa.int/> (5.1.2010).
- SATALINO, G., MATTIA, F., LE TOAN, T. & RINALDI, M., 2009: Wheat Crop Mapping by Using ASAR AP data. – *IEEE Transactions on Geoscience and Remote Sensing* **47**: 527–530.
- SCHOWENGERDT, R.A., 2007: Remote sensing: models and methods for image processing. – 3rd ed., Elsevier Academic Press, Amsterdam, The Netherlands.
- STILES, J., SARABANDI, K. & ULABY, F., 2000: Electromagnetic scattering from grassland – Part II: Measurement and modeling results. – *IEEE Transactions on Geoscience and Remote Sensing* **38**: 349–356.
- STRACHAN, I.B., PATTEY, E. & BOISVERT, J.B., 2002: Impact of nitrogen environmental conditions on corn as detected by hyperspectral reflectance. – *Remote Sensing of Environment* **80**: 213–224.
- THENKABAIL, P.S., SMITH, R.B. & DE PAUW, E., 2000: Hyperspectral vegetation indices and their relationships with agricultural crop characteristics. – *Remote Sensing of Environment* **71**: 158–182.
- THENKABAIL, P.S., ENCLONA, E.A., ASHTON, M.S. & VAN DER MEER, B., 2004: Accuracy assessment of hyperspectral waveband performance for vegetation analysis application. – *Remote Sensing of Environment* **91**: 354–376.
- TUCKER, C.J., 1979: Red and Photographic Infrared Linear Combinations for Monitoring Vegetation. – *Remote Sensing of Environment* **8**: 127–150.
- WOODHOUSE, I.H. (ed.), 2006: Introduction to Microwave Remote Sensing. – Taylor & Francis, Boca Raton, New York, USA.
- XAVIER, A.C., RUDORFF, B.F.T., MOREIRA, M.A., ALVARENGA, B.S., DE FREITAS, J.G. & SALOMON, M.V., 2006: Hyperspectral field reflectance measurements to estimate wheat grain yield and plant height. – *Science Agriculture* **63**: 130–138.
- ZHAO, D., HUANG, L., LI, J. & QI, J., 2007: A comparative analysis of broadband and narrowband derived vegetation indices in predicting LAI and CCD of a cotton canopy. – *ISPRS Journal of Photogrammetry & Remote Sensing* **62**: 25–33.

Addresses of the Authors:

WOLFGANG KOPPE, Astrium GEO-Information Services, D-88039 Friedrichshafen, Tel.: +49-7545-84226, e-mail: wolfgang.koppe@astrium.eads.net or Institute of Geography, GIS & RS Group, University of Cologne, D-50923 Köln.

SIMON HENNIG, Astrium Geoinformation Services, D-88039 Friedrichshafen, Tel.: +49-7545-82995, e-mail: simon.hennig@astrium.eads.net

Dr. FEI LI, College of Resources and Environmental Sciences, China Agricultural University, CN-

100094, Beijing and College of Ecology and Environmental Science, Inner Mongolia Agricultural University, CN-010019, Hohhot, Tel.: +86-471-4307376, e-mail: cau_lifei@163.com

MARTIN GNYP, Institute of Geography, GIS & RS Group, University of Cologne, D-50923 Köln, Tel.: +49-221-470-6620, e-mail: mgnypl@uni-koeln.de

Dr. YUXIN MIAO, Agro-Informatics and Sustainable Development Group, College of Resources and Environmental Sciences, China Agricultural University, CN-100193 Beijing, e-mail: ymiao@cau.edu.cn

Dr. LIANGLIANG JIA, Institute of Agricultural Resources & Environment, Hebei Academy of Agri-

culture and Forestry Sciences, CN-050051 Shijiazhuang, e-mail: jjiall@cau.edu.cn

Prof. Dr. XINPING CHEN, Department of Plant Nutrition, College of Resources & Environmental Sciences, China Agricultural University, CN-100094 Beijing, e-mail: chenxp@cau.edu.cn

Prof. Dr. GEORG BARETH, Institute of Geography, GIS & RS Group, University of Cologne, D-50923 Köln, Tel.: +49-221-470-6552, Fax: +49-221-470-1638, e-mail: g.bareth@uni-koeln.de

Manuskript eingereicht: Dezember 2011
Angenommen: März 2012